Solar forcing and El Niño-Southern Oscillation (ENSO) influences on productivity cycles interpreted from a late-Holocene high-resolution marine sediment record, Adélie Drift, East Antarctic Margin

E. Costa,[1] R.B. Dunbar,[1] K.A. Kryc,[1] D.A. Mucciarone,[1] S. Brachfeld,[2] E. B. Roark,[1] P.L. Manley,[3] R.W. Murray,[4] and A. Leventer[5]

[1]Department of Geological and Environmental Sciences, 325 Braun Hall, Stanford University, Stanford, CA, 94305, USA
[2]Department of Earth and Environmental Studies, Montclair State University, Montclair, NJ, 07043, USA.
[3]Department of Geology, Middlebury College, McCardell Bicentennial Hall 427, Middlebury, Vermont, USA
[4]Department of Earth Sciences, Boston University 675 Commonwealth Ave., Boston, MA 02215, USA
[5]Department of Geology, Colgate University, Hamilton, NY USA.

Abstract Core JPC17B was collected from the Adélie-Drift, a nearly 300-m thick drift deposit at 140ºE along the Indian Ocean sector of the Antarctic continental shelf. Sediments consist of nearly continuously laminated diatom mud and diatom ooze, with accumulation rates on the order of 20-21 m kyr^{-1} based on 10 AMS radiocarbon dates. Spectral analysis was performed on time series of opal content, $d^{13}C_{org}$, Ti content, and Ba content. Strong decadal to century-scale variability is present in all proxies. Opal and Ti-time series show strong variance at periods of 11, 22 and 110-years, which are suggestive of solar forcing. Ba-time series exhibits strong variance at a period of 3-3.6-yr, consistent with possible El Niño-Southern-Oscillation (ENSO) forcing.

Citation: Costa, E., R.B. Dunbar, K.A. Kryc, D.A. Mucciarone, S. Brachfeld, E. B. Roark, P.L. Manley, R.W. Murray, A.Leventer, Solar forcing and El Niño Southern Oscillation (ENSO) influences on productivity cycles interpreted from a late Holocene high-resolution marine sediment record, Adélie Drift, East Antarctic Margin– Online Proceedings of the 10th ISAES X, edited by A. K. Cooper and C. R. Raymond et al., USGS Open-File Report 2007-1047, Short Research Paper 036, 6 p.; doi:10.3133/of2007-1047.srp036

Introduction

The Southern Ocean is the site of strong air-sea-ice interactions that impact the entire globe. Constructing long records of these interactions requires very high-resolution archives that record decadal, annual, and even seasonal signals. Along the Antarctic margin, laminated diatom-mud and diatom oozes are the most promising recorders of these high frequency climate signals (Leventer et al., 1993, 1996, 2002, 2006; Pike et al., 2001; Bahk et al., 2003; Maddisson et al., 2005, 2006; Stickley et al., 2005; Denis et al., 2006). Here we present an ultra-high resolution record from the Indian Ocean sector of the East Antarctic Margin (Figure 1). The Adélie Drift (66.25'S, 140.25'E) was discovered and surveyed during cruise 01-01 of the United States Antarctic Program Research Vessel *Nathaniel B. Palmer* (hereafter NBP01-01). 3.5-kHz sub-bottom profiling and single-channel seismic profiling revealed a sediment accumulation nearly 300-m thick, the majority of which is likely Holocene in age. Sediment cores recovered from the drift are nearly continuously laminated (Crosta et al. 2005; Denis et al. 2006; Leventer et al., 2006), with sedimentation rates of 7.6 to 20 m kyr^{-1}. Here we compare downcore records of opal, $\delta^{13}C$, Ti and Ba content, and use time series analysis to investigate sedimentation cycles that are possibly forced by solar variability and El Niño Southern Oscillation (ENSO) influences (e.g., Christoforou & Hameed, 1997; Bertler et al., 2004).

Methods

The Adélie drift was cored during NBP01-01 (KC17, KC17B, JPC17B) (Leventer et al., 2006) and revisited with the 60-m CALYPSO corer during IMAGES cruise 03-2597 of the French Research Vessel Marion Dufrèsne

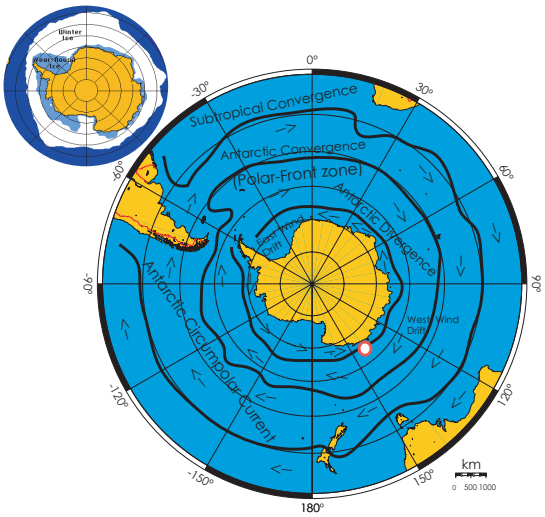

Figure 1. Antarctic Sea Ice margins: Mean winter sea-ice cover and year-round Antarctic ice measured from 1978-1987 with a passive-microwave satellite. Distribution of the atmospheric Polar Front, East and West wind drift driven by Polar Easterlies and Westerlies and the Antarctic currents (modified from Orsi et al. 1995 and Gloersen et al. 1992).The red point locates the core JPC17B (140.25'E, 66.25'S) (Adélie Drift).

(Crosta et al., 2005; Denis et al., 2006). Core JPC17B (66°24.852'S, 140°25.164'E, water depth = 1048m) is 26.5 m long and consists of diatom mud and laminated diatom ooze. Whole core sections were measured for magnetic susceptibility, gamma-ray attenuation (GRAPE) bulk density, and p-wave velocity on a Geotek Multisensor Track at the Antarctic Marine Geology

Research Facility at Florida State University. The core was then split, photographed, and described. All observed calcite macrofossils were collected for radiocarbon dating at Lawrence Livermore National Laboratory. Three bulk sediment samples were collected to date the acid insoluble organic matter (AIOM).

The working half of JPC17B was sub-sampled every 2 to 10 cm for physical properties, magnetic and geochemical analyses. Mass-normalized magnetic susceptibility (χ) was measured at 2.5-cm resolution using freeze-dried samples to remove the dilution effects of water. Samples were measured on an AGICO KLY-4 Kappabridge at Montclair State University. Samples for $\delta^{13}C_{org}$ and biogenic silica (opal) were taken at 2-cm intervals from 0 to 2 m, and every 10 cm from 2-m to the base of JPC17B. $\delta^{13}C_{org}$ was analysed on a Finnigan MAT Delta+ mass spectrometer interfaced with a Carlo-Erba series 1500 CN analyser at Stanford University. Biogenic silica analyses followed a protocol modified from Mortlock and Froelich (1989), in which biogenic silica is dissolved in a 0.5 M NaOH solution. Absorbance of the samples is measured every hour for 5 hours to build a dissolution curve. Absorbance is calibrated to weight % opal using five standards. Quality control is ensured by measuring replicate samples and blanks.

X-ray fluorescence (XRF) measurements were made using a CORTEX XRF core scanner at Bremen University. Titanium and barium content, expressed in normalized counts, were measured at 1-cm intervals from 1832 cm to 2649 cm, following the Jansen et al. 1998 method. This depth interval is marked by thinly to thickly bedded diatom ooze with noticeable differences in color and texture between the laminations. Barium is considered a reliable proxy of productivity and Ti is used as a proxy of clay mineral versus organic matter content (Yarincik and Murray, 2000). Spectral analysis of χ ,Ti and Ba XRF data, $\delta^{13}C$, and opal content was accomplished using the Singular Spectrum Analysis Toolkit SSA-MTM (Multi-Taper method) (Ghil et al., 2002). Three tapers were used for all MTM analyses. The temporal resolution of each time series was dependent on the spatial sampling resolution of each proxy, and equated to 0.5 years for the XRF data, and 5 years for opal and $\delta^{13}C_{org}$ data.

Results

Chronology

The chronology for core JPC17B is based on ten AMS radiocarbon samples (Table 1). AMS samples consist of acid insoluble organic matter (AIOM) and biogenic calcite from shells and shell fragments. We applied a reservoir correction of 1200 years based on corrections derived for AIOM and calcite ages in the Antarctic Peninsula and Ross Sea (Berkman and Forman, 1996). Corrected radiocarbon years were calibrated to calendar years B.P. using CALIB 5.0.2 (Stuiver et al., 2005).

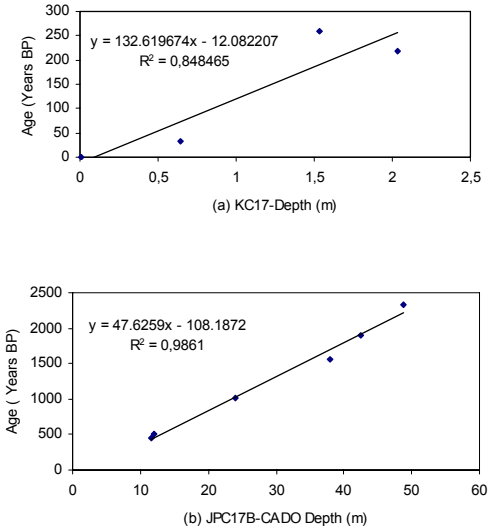

Figure 2. **(a)** Surface depth-age model based on four AIOM dates between 0 to 2.03 mcd. This subset of data yields a LSR of 7.6 m kyr^{-1}. **(b)** Deep depth-age model based on two AIOM (12.04 and 24.06 mcd) dates and four calcite dates between 11.53 to 48.72 mcd. AIOM dates has been adjusted by 400 years in order to merge the AIOM and calcite dates into one age model, with a LSR of 20-21 m kyr^{-1}

We calculated linear sedimentation rates (LSR) and constructed a depth-age model using 3 subsets of the age data. First, we fit a least squares line to the four AIOM dates between 0 to 2.03 mcd (Table 1). This subset of data yields a LSR of 7.6 m kyr^{-1}, and predicts an age of approximately 250 yr B.P. for 2 mcd. Next, we fit a least squares line to the three AIOM dates between 2.03 – 24.06 mcd, and lastly a least squares line to the four calcite dates between 11.73 – 48.72 mcd. These two line fits yield very similar sedimentation rates of 20-21 m kyr^{-1}. Although these two depth-age lines are nearly parallel, we observe that the AIOM line is offset towards older ages relative to the calcite line. At a given horizon, the AIOM age is approximately 325-400 years older than the calcite-derived age at that horizon. We suggest that this age offset results from the presence of old detrital carbon in the sediment, which skews dates derived from bulk sedimentary organic matter. Therefore, we have adjusted the AIOM dates by 400 years in order to merge the AIOM and calcite dates into one age model. The resulting age model applied to cores KC17 and JPC17B is as follows (Figure 2): surface age model: 0 to 2 mcd: $y = 132.6x - 12.1$; $R^2 = 0.84$. Deep age-model:11.53 to 48.72 mcd: $y = 47.6x - 108.2$; $R^2 = 0.98$ where y = age in years B.P. and x = depth in mcd.

Sedimentology and Geochemistry

The Adélie Drift sediments consist of thinly to thickly bedded diatom ooze, with laminations several mm to several cm thick. The cores are laminated over the

Table 1. Accelerator Mass Spectrometry ^{14}C ages from cores KC17, JPC17B and CADO core.

Core, interval (cm)	Composite Depth (mcd)	^{14}C age ± 1 sigma Corrected[b] (yrs BP)	Calibrated age (cal. BP)	Carbon source[a]
KC17, 0-2 cm	0.01	1800 ± 40	0	AIOM
KC17, 63-65 cm	0.64	1540 ± 40	33	AIOM
JPC17B,153-155 cm	1.53	1800 ± 35	258	AIOM
KC17, 202-204 cm	2.03	1770 ± 40	219	AIOM
JPC17B, 1152-1154 cm	11.53	2010 ± 35	456	calcite
JPC17B, 1203-1205 cm	12.04	2480 ± 40	831	AIOM
CADO8-11 2405-2407 cm	24.06	3000 ± 40	1335	AIOM
CADO8-11 3802-3804 cm	38.03	3195 ± 35	1557	calcite
CADO8-11, 4247-4259 cm	42.48	3485 ± 35	1896	calcite
CADO8-11, 4871-4873 cm	48.72	3855 ± 35	2339	calcite

[a] = acid insoluble organic matter; calcite denotes a shell fragment (*Lab. Code=LLNL)*

majority of their lengths, with only a few isolated intervals of bioturbated diatom mud. The biosiliceous, water-saturated nature of the sediment is evident in the physical properties measurements (Figures 3-4). Magnetic susceptibility is very weak, ranging from $0.07 – 5 \times 10^{-7}$ m^3 kg^{-1}. The weak values of χ reflect the high biogenic silica and low iron oxide contents of the sediment. The relationship between χ and biogenic silica varies down core. In some intervals χ is inversely correlated with biogenic silica. This is the usual and the expected relationship, in which diamagnetic silica dilutes the iron-bearing paramagnetic and ferrimagnetic particles contributed by terrigenous sediment. However, we also observe intervals where χ is positively correlated with biogenic silica. In these intervals we speculate that rapidly sinking phytoplankton detritus entrains silt and clay particles from the water column. If this true, then we would expect χ to be positively correlated with the clay-sized particle abundance. An alternate possibility is that these atypical intervals contain authigenic minerals that enhance magnetic susceptibility, possibly superparamagnetic magnetite, ferrimagnetic sulfides, paramagnetic Mn oxides, or paramagnetic clay minerals. Any of these would raise the overall χ value in a diatom ooze layer while having minimal impact on the iron content of the sediment. GRAPE-Bulk density values are low, ranging from 0.16 g cm^{-3} to 1.24 g cm^{-3}. The lowest values correspond with ooze laminations. Bulk density increases gradually with depth below 11 mcd, presumably due to sediment compaction. Opal content oscillates between 31 and 66% by weight, with an average value of 45%. Peak values (> 58 %) are observed in samples collected from ooze laminations. $\delta^{13}C_{org}$ ranges from -24.08 ‰ at 2551 cm to -30.17 ‰ at 250 cm, with an average value of -26.61 ‰ typical for Antarctic oozes (Crosta et al. 2005).

Ti, and Ba relative concentrations were measured by X-ray fluorescence between 18.32 m to 26.49 m and are expressed in normalized counts per second (Figure 4).

Spectral Analysis

Multi-taper method (MTM) time series analysis results for $\delta^{13}C_{org}$, Ti, and Ba from JPC17B are displayed in Figure 5. Opal and $\delta^{13}C_{org}$ MTM-spectral analyses were completed for the entire time series. The opal time series, a proxy for paleoproductivity, reveals strong concentrations of variance at 11, 22, and 110 years (Figure 5a). The $\delta^{13}C_{org}$ series shows variance concentrated mainly within the decadal band (11 to ~18 years) (Figure 5b). The Ti and Ba timer series encompass the time interval 766 to 1152 yr B.P. The Ti spectrum shows concentrations of variance at periods of 11 and 5-6 years (Figure 5c). The Ba spectrum shows variance concentrated within a relatively narrow 3 to 4 year period band (Figure 5d).

Discussion

The strong concentrations of variance at periods of 11, 22, and 110 years (opal) and 11-12 years (Ti) suggest a possible solar forcing effect. The two proxies are in fact related. Opal content reflects relative variations in the diatomaceous sediment flux to the seabed, as well as the supply of diluting terrigenous phases, tracked by elements by Ti and Al. Forcing at "solar" periods in Antarctica has been suggested previously. Centennial-scale variability has been documented in several proxies in the Palmer Deep record from the Antarctic Peninsula (Leventer et al., 1996; Domack et al., 2001), where the observed periodicities were consistent with those attributed to solar modulation of the radiocarbon production rate during the Holocene. Curran et al. 2003 studied the distribution of methanosulphonic acid (MSA) in the Law Dome (66º44'S, 112º50'E) ice core, near Adélie Land. Their results show a strong cyclicity at a period of 11 yr. Since MSA forms from marine-derived dimethyl sulphide, Curran et al. suggest that their ice core observations reflect variability in marine primary productivity along this sector of the East Antarctic margin. The East Antarctic Region (80°E to 140°E) is influenced by the southern boundary of the Antarctic Circumpolar Current (ACC), which in turn controls the northern extent of sea ice and therefore net biological productivity (Figure 1).

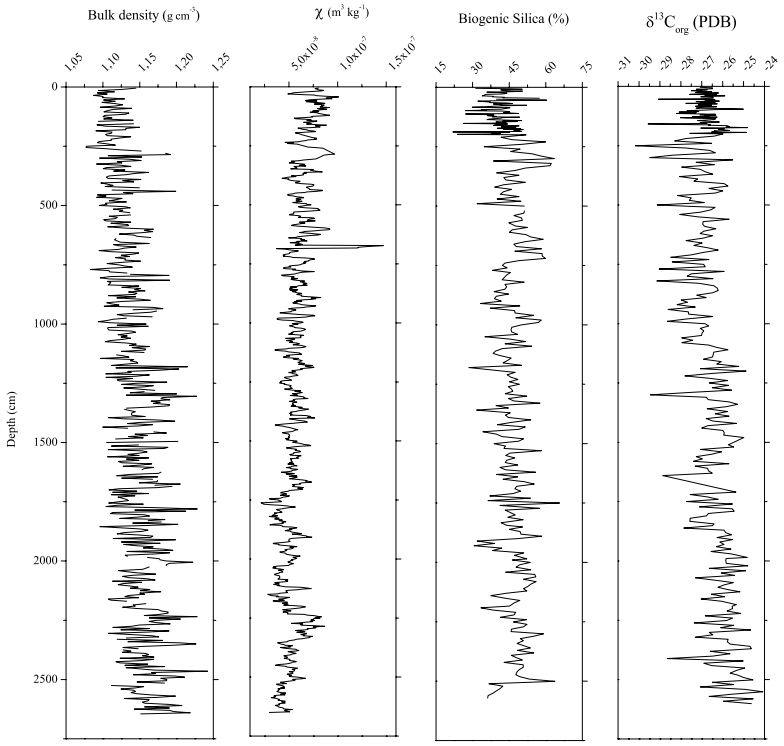

Figure 3. Down-core records in core JPC17B versus depth. Mass-normalized magnetic susceptibility (χ) data plotted in m^3 kg^{-1} after application of a five point smoothing function. χ average content is 5.70·10-8 m3 kg-1. Gamma-ray attenuation (GRAPE) bulk density average is 1.14 g cm^{-3}. The Biogenic silica average content is 45.03 (%). $\delta^{13}C_{org}$ has an average value of -26.61 ‰

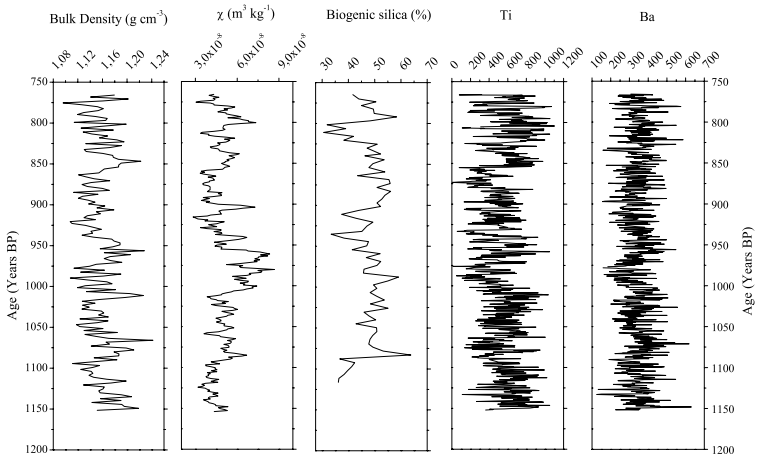

Figure 4. Down-core records in core JPC17B versus age. Bulk density (g cm-3) is samples every 2.38 yr (5 cm). Ti and Ba (XRF data in normalized cps.) are sampled in a time step of 0.47 yr (1 cm). Magnetic susceptibility (χ mass-normalized (m^3 kg^{-1}) is sampled every 1.19 yr (2.5 cm), and Opal (%) and δ^{13}Corg every 4.76 yr (10 cm).

Curran et al. 2003 suggest that solar cycles may play an important role controlling the variability in the southern boundary of the ACC. We suggest that the Adélie Drift sediment record shows similar variations in productivity, possibly controlled by sea ice extent, and modulated at solar periods. Christoforou and Hameed, 1997, described the influence of the 11-year solar cycle in the North Pacific. Using instrumental data they examined variations

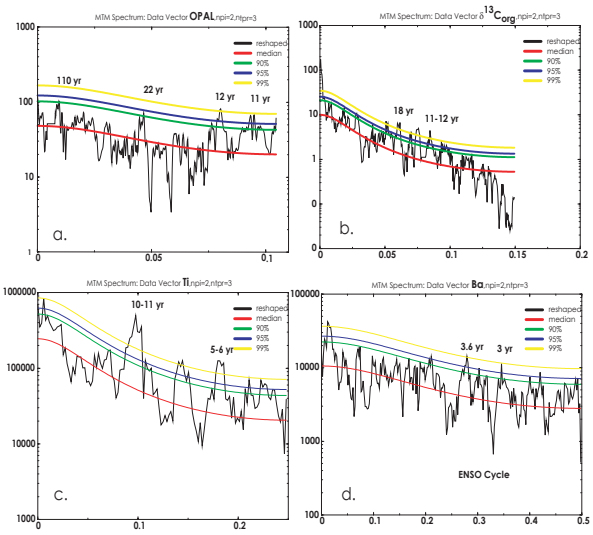

Figure 5. Multi-taper method (MTM) spectral power plots of proxies from JPC17B **(a)** Biogenic silica and **(b)** $\delta^{13}C_{org}$ for the interval 750 – 1150 yr BP, **(c)** Titanium and **(d)** Barium for the interval 750 – 1150 yr BP. We used three tapers and a time-step of 5 years in Opal and $\delta^{13}C_{org}$ data, and a time step of 0.5 years in the XRF data. Numbers above the reshaped and harmonic spectra are the periods of the most specific spectral peaks, rising above the 95% or 99% confidence limit

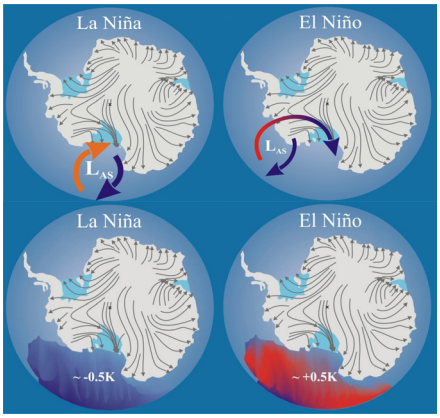

Figure 6. Size and position of the Amundsen Sea Low (L_{AS}). Thickness of the arrows (red color=warm air and in blue=cooler air) indicate strength of the L_{AS} during the el Niño & la Niña events. During la Niña a cooling is observed in Amundsen and Ross Sea. In contrast the region shows a warming during el Niño events. Grey arrows indicate katabatic wind flow (From Bertler *et al.* 2006).

in the semi-permanent pressure systems of the Aleutian Low and the Hawaiian High. Their results show a strong correlation between the locations of these pressure centers and solar variability, with significant longitudinal displacement of the Aleutian Low between solar maximum and minimum intervals. There is no equivalent instrumental data set that allows us to examine this same phenomena in the Southern Ocean, but it seems reasonable to expect a similar variation in large-scale atmospheric forcing there. We suggest that similar shifts in the Southern Hemisphere displace subpolar pressure centers as a function of solar forcing, with follow-on effects on the westerly wind field and circumpolar circulation regime (Figure 1).

The Ba time series shows concentrations of variance at periods consistent with teleconnections to the El Niño-Southern Oscillation (ENSO) (Figure 5d). The Ti data are likely showing a regional provenance signal that will vary with local glacial and sea ice conditions and might not be influenced by ENSO. If the Ba signal is indeed tracking productivity, this signal would be more easily influenced by global teleconnections resulting from ENSO variability. ENSO impacts sea surface temperatures (SSTs) in the central and eastern equatorial Pacific and has been suggested as an important driver of Antarctic climate and oceanic variability in an interannual to interdecadal timescales (Cullather et al., 1996; Bertler et al., 2004). One region where the ENSO global teleconnection appears particularly strong is in the high southern latitudes, in the South Pacific Ocean. El Niño has been detected in the Amundsen Sea (Kwok and Comiso, 2002), Ross Sea (Cullather et al., 1996; Ribera & Mann, 2003; Turner 2004) and in the Antarctic Pacific Sector (Chen et al, 1996; Jacobs et al., 2002; Turner, 2004), causing a warming effect. Bertler et al. 2004, 2006 reported an El Niño-ENSO warming of the eastern Ross Sea as a direct response to warmer sea surface temperatures and an apparently contradictory cooling of the western terrestrial Ross Sea region linked to an ENSO driven shift in the regional atmospheric circulation (Amundsen Sea Low, L_{AS}), originating in the Amundsen Sea and West Antarctica (Figure 6).

Conclusions

We present a multi-proxy record from a high resolution marine sediment sequence from the Adélie Drift, East Antarctica. Significant peaks in spectral power at periodicities of 10-12, 22, and 110 years are present in paleoproductivity proxies from the site, suggesting that solar variability influences exert a strong control on the Antarctic coastal climate and phytoplankton productivity during the late-Holocene. Spectral analysis of Ba content for the time interval 766 – 1152 BP reveals variance at a period of 3 to 4 yr, consistent with ENSO forcing during this time interval.

Acknowledgements. This project is funded by the National Science Foundation grants 9909367, 9909803, 9909793, 9909837, 0126110, and the Spanish postdoctoral fellowship Fundacion Ramon Areces. We also thank the ISAES X Co-editor D. K. Fütterer and A. K. Cooper (lead editor) for their revisions, comments & organization.

References

Bahk, J.J., Yoon H.I., Kim Y., Kang C.Y. and S.H. Bae (2003). Microfabric analysis of laminated diatom ooze (Holocene) from the

eastern Bransfield Strait, Antarctica Peninsula. *Geosciences Journal* 7, 135-42.

Berkman, P.A. and S.L. Forman (1996). Pre-bomb radiocarbon and the reservoir correction for calcareous marine species in the Southern Ocean. *Geophysical Research Letters* 23, 4; 363-366

Bertler, N.A.N., Barrett P.J., Mayewski P.A., Fogt R.L., Kreutz K.J. and J. Shulmeister (2004). El Niño suppresses Antarctic warming. *Geophysical research Letters* 31, L15207

Bertler, N.A.N, Niash, T.R., Mayewski, P.A. and P.J. Barrett (2006). Opposing oceanic and atmospheric ENSO influences on the Ross Sea Region, Antarctica. *Advances in Geosciences* 6, 83-86. Bertler, N.A.N., Oerter, H., Kipfstuhl, S., Barret, P.J., Naish, T.R. and Mayewski, P.A. (2006). The effects of joint ENSO-Antarctic Oscillation forcing on the McMurdo Dry Valleys, Antarctica. *Antarctic Science* 18, 507–514.

Chen, B., S. R. Smith, and D. H. Bromwich (1996). Evolution of the tropospheric split jet over the South Pacific Ocean during the 1986 – 1989 ENSO cycle. *Mon. Weather Rev.* 124, 1711– 1731.

Christoforou, P., and S. Hameed (1997). Solar cycle and the Pacific 'centers of action' (1997). *Geophys. Res. Lett.* 24(3), 293-296, 10.1029/97GL00017.

Crosta, X., Crespin J., Billy, I. and O. Ther (2005). Major factors controlling Holocene δ^{13}Corg change in a seasonal sea-ice environment, Adélie Land, East Antarctica. *Global Biogeochemical Cycles* 19, GB40299, doi:10.1029/2004GB002426.

Cullather, R.I., D.H. Bromwich, and M.L. Van Woert, 1996: Interannual variations in Antarctic precipitation related to El Niño-Southern Oscillation. *J. Geophys. Res.* 101, 19,109-19,118.

Curran M. A. J., Van Ommen T. D., Morgan V. I., Phillips K.L. and A.S. Palmer (2003). Ice Core Evidence for Antarctic Sea Ice Decline Since the 1950s. *Science* 302, 1203-1205.

Denis, D., Crosta X., Zaragosi S., Romero O., Martin B., and V. Mas (2006). Seasonal and subseasonal climate changes recorded in laminated diatom ooze sediments, Adélie Land, East Antarctica. *The Holocene* 16(8), 1137-1147.

Domack, E.W., Jull, A.J.T., Anderson, J.B., Linick, T.W., and Williams, C.R., 1989, Application of tandem accelerator mass-spectrometer dating to late-Pleistocene-holocene sediments of the east Antarctic continental shelf. *Quaternary Research* 31, 277-287.

Domack, E.W. and P.A. Mayewski (1999). Bi-polar ocean linkages: evidence from late-Holocene Antarctic marine and Greenland ice-core records. *The Holocene* 9(2), 247-251.

Domack, E.W., Leventer A., Dunbar R., Taylor F., Brachfeld S., Sjunneskog C. and ODP Leg 178 Scientific Party (2001). Chronology fo thePalmer Deep site Antarctic Peninsula: a Holocene palaeoenvironmental reference for the circum-Antarctic. *The Holocene*, 11(1), 1-9.

Domack, E., Duran, D., Leventer, A., Ishman, S., Doane, S., McCallum, S., Amblas, D., Ring, J., Gilbert, R., and M. Prentice (2005). Stability of the Larsen B ice shelf on the Antarctic Peninsula during the Holocene epoch. *Nature* 436, 681-685.

Ghil M., R. M. Allen, M. D. Dettinger, K. Ide, D. Kondrashov, M. E. Mann, A. Robertson, A. Saunders, Y. Tian, F. Varadi, and P. Yiou, (2002). Advanced spectral methods for climatic time series. *Rev. Geophys.* 40(1), 3.1-3.41, 10.1029/2000RG000092.

Gloersen P., Cambell W.J., Cavalieri D.J., Comiso J.C., Parkinson C.L., and Zwally H.J. (1992). Arctic and Antarctic Sea Ice, 1978-1987: satellite passive-microwave observations and analysis, *NASA* SP-511, *National Aeronautics and Space Administration*.

Jacobs, S. S., C. F. Giulivi, and P. A. Mele (2002), Freshening of the Ross Sea during the late 20th century, *Science*, 297, 386–389.

Jansen, J.H.F., Van der Gaast, S.J., Koster, B. and Vaars, A.J. (1998). CORTEX, a shipboard XRF-scanner for element analyses insplit sediment cores. Marine Geology 151, 143-153.

Kwok, R., and J. C. Comiso (2002), Spatial patterns of variability in Antarctic surface temperature: Connections to the Southern Hemisphere Annular Mode and the Southern Oscillation, *Geophys. Res. Lett.* 29(14), 1705.

Leventer, A., Dunbar, R. B., and DeMaster, D. J., 1993, Diatom evidence for late Holocene climatic events in Granite Harbor, Antarctica: *Paleoceanography* 8, 373–386.

Leventer, A., Domack E.W., Ishman S.E., Brachfeld S., McClennen C.E. and P. Manley (1996). Productivity cycles of 200-300 years in the Antarctic Peninsula region: Understanding linkages among the sun, atmosphere, oceans, sea ice and biota. *GSA Bulletin* 108(12), 1626-1644

Leventer, A., Domack, E., Barkoukis, A., McAndrews, B., and Murray, J. (2002). Laminations from the Palmer Deep: a diatom-based interpretation, *Paleoceanography* 17(3), 1-15.

Leventer, A., Domack, E., Dunbar, R., Pike, J., Stickely, C., Maddison, E., Brachfeld, S., Manley, P. and C. McClennen (2006). Marine sediment record from the East Antarctic margin reveals dynamics of ice sheet recession. *GSA Today* 16, 4-10.

Maddison, E.J., Pike, J., Leventer, A. and Domack, E.W. 2005: Deglacial seasonal and sub-seasonal diatom record from Palmer Deep, Antarctica. Journal of *Quaternary Science* 20, 435-46.

Maddison, E.J., Pike, J., Leventer, A., Dunbar, R., Brachfeld, S., Domack, E.W., Manley, P., and C. McClennen (2006). Post-glacial seasonal diatom record of the Mertz Glacier polynya, East Antarctic, *Marine Micropaleontology* 60(1), 66-88.

McMullen, K., Domack, E., Leventer, A., Dunbar, R. and S. Brachfeld (2006). Glacial morphology and marine stratigraphy of the Mertz Trough, East Antarctica, *Paleoceanography, Palaeoclimatology, Palaecology* 231, 169-180.

Meyerson, E. A., Mayewski, P. A., Kreutz, K. J., Meeker, L. D., Whitlow, S. I., and Twickler, M. S. (2002). The polar expression of ENSO and sea-ice variability as recorded in a South Pole ice core. *Ann.. Glaciol.* 35, 430–436.

Mortlock R.A. and P.N. Froelich (1989). A simple method for the rapid determination of biogenic opal in pelagic marine sediments. *Deep-sea res. Part A, Oceanogr. res. pap.* 36(9), 1415-1426

Orsi, A.H., Whitworth III, T., and W. D., Nowlin Jr (1995). On the meridional extent and fronts of the Antarctic Circumpolar Current. *Deep-Sea Research I* 42 (5), 64-673.

Pike, J., Moreton, S.G. and Allen, C.A. 2001: Data report: microfabric analysis of postglacial sediments from Palmer Deep, Western Antarctic Peninsula. In Barker, P.F., Camerlenghi, A., Acton, G.D. and Ramsay, A.T.S., editors, Proceedings of the ODP. *Science Research* 178, 1-17.

Pudsey, C. J., Barker, P. F., and Larter, R. D., 1994, Ice sheet retreat from the Antarctic Peninsula shelf. *Continental Shelf Research* 14, 1647–1675.

Ribera, P., and M. E. Mann (2003). ENSO related variability in the Southern Hemisphere, 1948–2000. *Geophys. Res. Lett.* 30(1), 1006, doi:10.1029/2002GL015818.

Stickley, C.E., Pike, J., Leventer, A., Dunbar, R., Domack, E.W., Brachfeld, S., Manley, P., and C. McClennen (2005). Deglacial ocean and climate sensitivity in laminated diatom sediments, Mac.Robertson Shelf, Antarctica, *Paleoceanography, Palaeoclimatology, Palaecology* 227, 290-310.

Sonnett, C.P., and Finney, S.A. (1990). The spectrum of radiocarbon: Philosophical Transactions. *Royal Society of London* 30A, 413–426.

Stuiver M. and T.F. Braziunas (1993). ^{14}C Ages of Marine Samples to 10,000 BC. *Radiocarbon* 35(1), 137-189.

Turner, J. (2004). Review: The El Niño-Southern Oscillation and Antarctica. *Int. J. Climatol.* 24, 1-31.

Yarincik, K.M. and Murray, R.W. (2000). Climatically sensitive eolian and hemipelagic deposition in the Cariaco Basin, Venezuela, over the past 578,000 years: results from Al/Ti and K/Al. *Paleoceanography* 15, 210-228.